Doping-induced topological phase transition in Bi: The role of quantum electronic stress

Kyung-Hwan Jin,[1] Han Woong Yeom,[2,3] and Feng Liu[1,*]

[1]*Department of Materials Science and Engineering, University of Utah, Salt Lake City, Utah 84112, USA*
[2]*Center for Artificial Low Dimensional Electronic Systems, Institute for Basic Science (IBS), Pohang 37673, Republic of Korea*
[3]*Department of Physics, Pohang University of Science and Technology, Pohang 37673, Republic of Korea*

(Received 9 July 2019; revised manuscript received 10 December 2019; published 8 January 2020)

Charge doping is an essential means to tailor a materials' properties. However, besides moving the Fermi level, charge doping is generally not expected to induce topological phase transition (TPT). Here, using first-principles calculations, we demonstrate an electron doping-induced TPT in bulk Bi from a higher-order topological insulator (HOTI) to a TI. The underlying mechanism is revealed to be driven by an electron doping-induced quantum electronic stress (QES), which in turn induces a highly anisotropic lattice expansion to close/reopen the small energy gap in Bi band structure. Our finding significantly resolves an outstanding controversy concerning the topological characterization of bulk Bi among existing experiments and theories, and explains the physical origin of the topological order in Bi (111) thin films. It sheds new light on the fundamental understanding of topological properties of small band gap materials in relation to doping and QES.

DOI: 10.1103/PhysRevB.101.035111

I. INTRODUCTION

Charge doping affords a versatile approach to modify electronic properties of solid materials [1,2]. In particular, doping plays a critical role in modern electronics technologies, as *p-n* junctions are elementary "building blocks" for semiconductor devices such as diodes, transistors, and solar cells. It is also well known that charge doping induces superconductivity in various materials such as high-T_c superconductors [3], charge-density-wave materials [4], and more recently, graphene [5,6] and topological insulators (TIs) [7,8]. For TIs, doping plays an obvious role to move the Fermi level into the topological gap in many theoretically predicted "extrinsic" TIs [9–12] and controls the sign and density of topologically protected charge carriers. That is, doping in topological materials has largely been treated within the rigid-band model, i.e., moving the topological band structures up and down in energy without significantly modifying band structure. Therefore, doping is generally not expected to alter the topological property of the materials itself.

In this work we demonstrate that electron doping unexpectedly induces a TPT, such as in bulk Bi from a higher-order topological insulator (HOTI) to a TI, which is one of the most important and fundamental TIs with technological implication for the quantum spin Hall [13–15] and Majorana devices [16]. We further show that this surprising transition is driven by an electron doping-induced quantum electronic stress (QES) [17], which in turn brings about a sizable anisotropic compressive lattice strain that expands the interlayer spacing and closes (and reopens) a small energy gap at the L point ($\sim$10$-$20 meV) in the Bi band structure. Our finding resolves an outstanding controversy concerning the precise topological property of bulk Bi among existing experiments and theories, and explains the physical origin of the intriguing topological order in Bi (111) thin films. This work clearly provides an extra control knob into the topological nature of small gap materials.

Bismuth, a widely studied low-density semimetal with strong spin-orbit coupling (SOC), shows a wealth of intriguing quantum phenomena like diamagnetism [18], electron fractionalization [19], and unconventional superconductivity [20]. In spite of the enormous amount of research, the topological classification of Bi has remained controversial. Early theoretical models and calculations indicate that bulk Bi possesses a trivial Z_2 topological order [21–26], while a recent study showed it is a HOTI which is consistent with the principal trivial band order [27]. In contrast, angle-resolved photoemission spectroscopy (ARPES) measurements on Bi (111) surfaces indicated that Bi bulk has a nontrivial topology [28–32]. Such discrepancy makes it difficult for further studies, in particular in attempts to resolve hinge mode of HOTI [27] and Majorana zero modes of heterostructure of Bi film and superconductor [33]. While previous theoretical calculations were done only for intrinsic Bi, our calculations show that the level of electron doping and hence the amount of QES in experimental samples can actually change the topological order of Bi. As a striking consequence, a very good agreement between the ARPES data and the calculated topological surface states of the (111) surface has been achieved after considering electron doping.

QES is generally defined as a nonmechanical form of lattice stress induced by pure electronic excitation and perturbation in the absence of lattice strain [17]. For the case of doping, it displays a linear dependence on the amount of doping, following the so-called quantum Hooke's law [17,34]:

$$\sigma^{\mathrm{QE}} = \Xi \Delta n, \tag{1}$$

where Ξ is the deformation potential and Δn is the change of electron density. In general, electron (hole) doping induces a compressive (tensile) QES that expands (contracts) the lattice

*Corresponding author: fliu@eng.utah.edu

 ©2020 American Physical Society

[17]. For bulk Bi, our calculations show that electron doping induces a highly anisotropic QES. It predominantly expands the interlayer spacing between the (111) planes, which is consistent with an intermediate interlayer bonding strength [35–37]. This will in turn close/reopen the gap at the L point and induces a band inversion for topological transition. Thus, different amounts of electron doping can lead to different topological phases, which we reveal to be responsible for the previous controversial observations [21–32].

II. COMPUTATIONAL METHOD

We performed first-principles calculations within the framework of density-functional theory, as implemented in the Vienna *ab initio* simulation package [38,39]. All the calculations are performed using the cutoff of 400 eV on a $15 \times 15 \times 15$ Monkhorst-Pack k-point mesh. All structures are fully optimized until the residual forces are less than 0.01 eV/Å. The van der Waals (vdW) interaction in the Tkatscenko-Scheffler [40] together with SOC was included. The modified Becke-Johnson (mBJ) exchange potential [41,42] and HSE06 [43] was employed to obtain a more accurate electronic band of bulk Bi. We further calculate the surface density of states and Fermi surface using the Wannier-basis surface Green's function method [44–46].

III. RESULTS AND DISCUSSION

Bulk Bi crystallizes with a rhombohedral structure belonging to the space group $R\bar{3}m$ (166) [47]. Figure 1(a) shows its unit cell indicated by cyan lines with two Bi atoms. It has a bilayered structure, with an ABC stacking sequence along the (111) direction. The corresponding bulk and surface Brillouin zone (BZ) are presented in Fig. 1(b). One Bi (111) bilayer forms a buckled hexagonal lattice [Fig. 1(c)]. There are three key structural parameters to define the bulk lattice: The (111) in-plane lattice constant a, the (111) bilayer buckling height b, and interbilayer spacing c. For the reference lattice, we used experimental parameters [48] with $a_{eq} = 4.546$ Å, $b_{eq} = 1.640$ Å, and $c_{eq} = 2.314$ Å (equivalently, $a_{rh} = 4.746$ Å, $d_1/d_2 = 0.893$, and $\alpha = 57.230°$ viewed in the rhombohedarl lattice). The (110) surface has a quasisquare unit cell, and each layer consists of two sublayers with a small buckling [Fig. 1(d)]. The effect of electron doping is simulated by adding electrons to the intrinsic Bi lattice with a compensating uniform positive charge background.

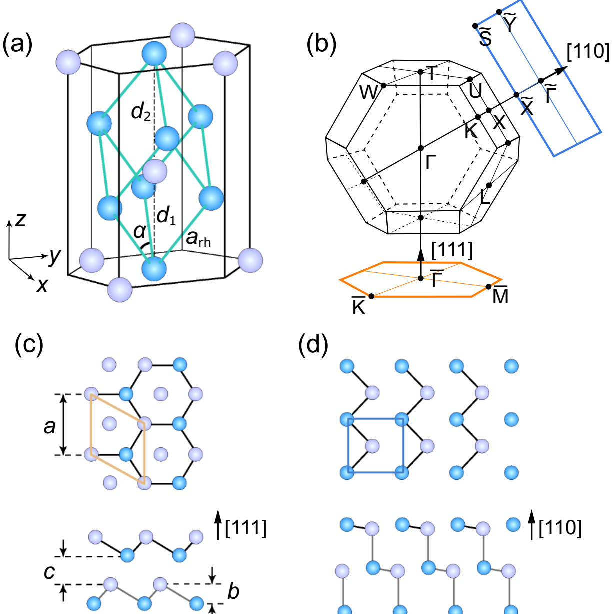

FIG. 1. (a) Rhombohedral (cyan) unit cell and hexagonal crystal structure (black) of Bi bulk. (b) Brillouin zone of the Bi bulk and surface in the [111] and [110] directions. Top and side view of (c) Bi (111) and (d) Bi (110) surfaces. The unit cell of the Bi (111) and Bi (110) surfaces is indicated by a yellow rhombus and a blue rectangle, respectably.

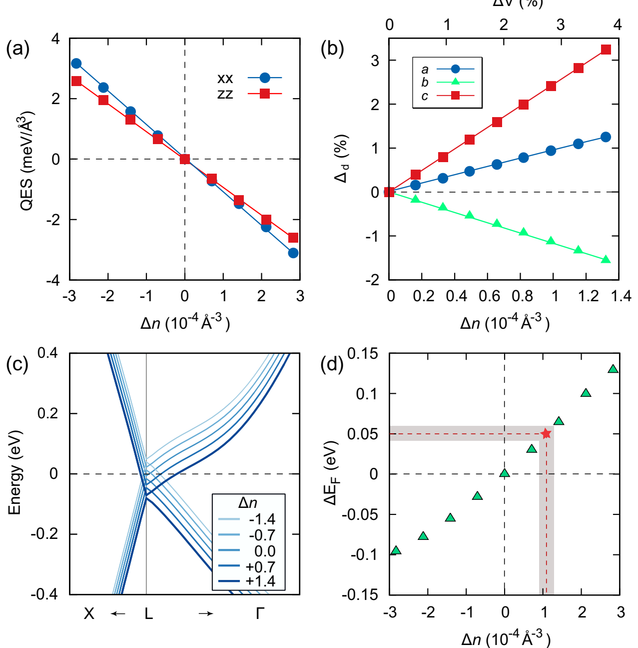

FIG. 2. (a) The QES as a function of the variation of carrier density Δn. (b) The change of lattice volume, the (111) in-plane lattice constant a, the bilayer buckling height b, and interbilayer spacing c, as a function of Δn. (c) Band structure of Bi bulk near the L point varying with carrier density Δn and (d) corresponding Fermi level shift (ΔE_F). The shift of $\Delta E_F = 0.05$ eV as marked by star corresponds to electron density $\Delta n \sim 1.1 \times 10^{-4}/\text{Å}^3$.

We first investigated the compressive QES induced by electron doping in bulk Bi, which in turn induces a lattice expansion [17]. In general, electron doping does not change crystal lattice symmetry, but induces an anisotropic QES and hence an anisotropic strain, in accordance with the lattice symmetry. Figure 2(a) shows the calculated QES ($\boldsymbol{\sigma}^{QE}$) as a function of the doped electron density (Δn) in the equilibrium Bi lattice. The components of QES (σ_{xx} and σ_{zz}) are taken from the diagonal elements of an anisotropic stress tensor, since Bi has an anisotropic lattice structure. One can clearly see the linear dependence of $\boldsymbol{\sigma}^{QE}$ on Δn as expected from Eq. (1), from which we extract an anisotropic deformation potential $\Xi_{xx} = -10.97$ eV and $\Xi_{zz} = -9.25$ eV. Next, we

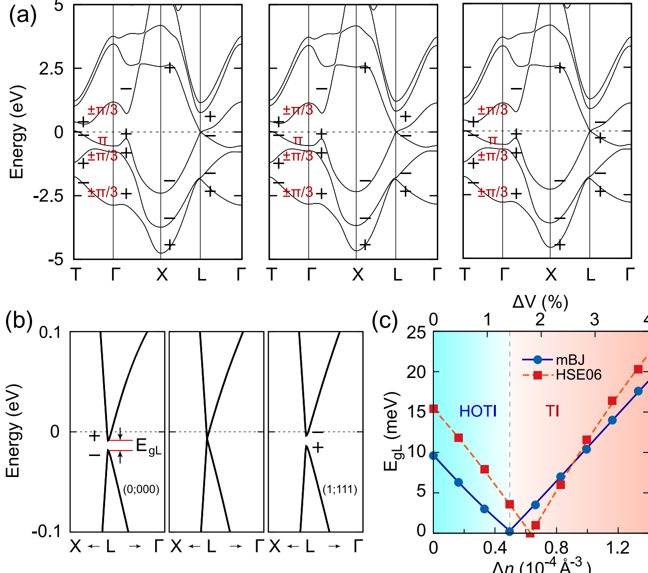

FIG. 3. (a) Calculated band structure for intrinsic Bi, doped with $\Delta n = 0$, $0.49 \times 10^{-4}/\text{Å}^3$, and $0.98 \times 10^{-4}/\text{Å}^3$ ($\Delta V = 0\%$, 1.4%, and 2.8%), respectively. Parity ($\hat{C}_3$) eigenvalues are indicated by + and − (π and $\pm\pi/3$) signs. (b) Enlarged band structures of (a) near the L point. (c) Band gap at the L point as a function of Δn (or optimized volume) using mBJ and HSE06 functionals.

determined the amount of lattice expansion induced by electron doping, by optimizing the lattice structure to eliminate the QES, as shown in Fig. 2(b). The lattice (ΔV) expands linearly with Δn, but in a highly anisotropic fashion, in particular the (111) interbilayer spacing c increases much more than the in-plane lattice constant a, while the bilayer buckling height b actually decreases [Fig. 2(b)]. This is resulted from both the anisotropic QES and the anisotropic elastic constants of Bi ($C_{11} = 69.3$ and $C_{33} = 40.4$) [49,50]. Physically it implies that electron doping will predominantly increase the interlayer spacing of Bi (111) thin films, which is known to have an intermediate bonding strength between weak vdW and strong chemical bonding [35–37].

We also checked the band evolution near the L point and the corresponding Fermi level shift as a function of electron doping. It is confirmed that the electron (hole) doping leads to a constant upward (downward) shift of the Fermi level without altering significantly the band dispersion, validating the rigid-band approximation [see Fig. 2(c)]. Since the electron states of bulk Bi near the Fermi level are all in one band, separated in energy from the other bands, the rigid-band model is reasonable. The shift of Fermi level (ΔE_F) is shown in Fig. 2(d) as a function of Δn, with the $\Delta E_F = 0.05$ eV marked for $\Delta n \sim 1.1 \times 10^{-4}/\text{Å}^3$ to be discussed further later.

Figure 3(a) show the whole band structure of bulk Bi at three optimized lattices, $\Delta V = 0\%$, 1.4%, and 2.8%, corresponding to $\Delta n = 0$, $0.49 \times 10^{-4}/\text{Å}^3$, and $0.98 \times 10^{-4}/\text{Å}^3$, respectively, within the rigid-band approximation without shifting Fermi energy. Figure 3(b) shows the enlarged band structure of Fig. 3(a) near the L point for clarity. The semimetallic character of bulk Bi is maintained upon electron doping. Depending on doping level, there could be an electron pocket located at L point and/or hole pocket at the T point. The band gap at the L point for intrinsic Bi is quite small ($\leqslant 20$ meV) which is considered to be the origin of the controversial topological classification of bulk Bi [32]. As the electron doping increases, the band gap at the L point decreases and importantly closes at a critical point, and then reopens [Fig. 3(b)]. This indicates a TPT at $\Delta n_c \sim 0.49 \times 10^{-4}/\text{Å}^3$ [Fig. 3(c)]. The critical doping concentration (volume expansion) for the HOTI-to-TI transition is $\Delta n_c \sim 0.62 \times 10^{-4}/\text{Å}^3$ (1.8%) obtained from the HSE06 functional, which is slightly larger than that obtained from the mBJ calculation ($0.49 \times 10^{-4}/\text{Å}^3$).

To identify the topological phase clearly, two topological invariants ($\nu^{(\pi)}$ and $\nu^{(\pm\pi/3)}$) in the occupied subspaces with $\hat{C}_3$ rotation symmetry [eigenvalues -1 and $\exp(\pm i\pi/3)$] are used to account for total band inversion [27]. They are given by

$$\nu^{(\pi)} = \nu_\Gamma^{(\pi)} \nu_T^{(\pi)} \nu_X \nu_L, \qquad \nu^{(\pm\pi/3)} = \nu_\Gamma^{(\pm\pi/3)} \nu_T^{(\pm\pi/3)}, \qquad (2)$$

respectively. There are three possible cases: $\nu^{(\pi)} = \nu^{(\pm\pi/3)} = +1$ indicates a normal insulator; $\nu = \nu^{(\pi)}\nu^{(\pm\pi/3)} = -1$ indicates a TI; and $\nu^{(\pi)} = \nu^{(\pm\pi/3)} = -1$ indicates a HOTI. Note that ν is a Z_2 topological index. For bulk Bi there exists a direct band gap separating the valence bands from conduction bands in the whole k space, which allows for an unambiguous definition of the topological invariant. The crystal structure of Bi has inversion symmetry, so for each band one can define the parity eigenvalues (± 1) of the occupied bands at time-reversal invariant momenta (TRIM) points [51]. Here we can evaluate the $\nu^{(\pi)}$ and $\nu^{(\pm\pi/3)}$ for the occupied bands. Specifically, along the Γ-T line, $\hat{C}_3$ eigenvalues are -1 and $\exp(\pm i\pi/3)$ for spin-1/2 particles, as indicated by red marks in Fig. 3(a); they are unchanged with electron doping. Below the critical concentration ($\Delta n < \Delta n_c$) $\nu^{(\pi)} = \nu^{(\pm\pi/3)} = -1$, indicating a HOTI [27]. The Z_2 index is 0 due to double band inversion at L point, but the $\hat{C}_3$-graded double band inversion at T point ($\nu_T^{(\pi)} = \nu_T^{(\pm\pi/3)} = -1$) gives rise to the HOTI phase. Above the critical concentration ($\Delta n > \Delta n_c$), the indices change to $\nu^{(\pi)} = 1$ and $\nu^{(\pm\pi/3)} = -1$, indicating a TI ($\nu = -1$). The band inversion occurs only once at the L point. The process of such electron doping-induced TPT in bulk Bi is clearly illustrated in Fig. 3(c) using mBJ and HSE06 functionals.

Different topological phases are characterized with different forms of surface states. Figure 4(a) shows the calculated band structure of Bi (111) thin films of 10 bilayer (BL), 40 BL, and 100 BL thickness in comparison with the semi-infinite surface for the HOTI phase without doping ($\Delta n = 0$). Figure 4(b) shows the same for the TI phase with electron doping ($\Delta n = 0.98 \times 10^{-4}/\text{Å}^3$). Without doping [Fig. 4(a)], as the thickness increases, the two surface branches converge and become degenerate at $\overline{M}$, forming a surface Dirac cone. There are an even number of Dirac cones, one at $\overline{\Gamma}$ and three at $\overline{M}$, consistent with the HOTI band topology. In contrast, with doping [Fig. 4(b)], the semi-infinite surface bands display a nontrivial band topology; the two surface branches merge into conduction and valence bands separately as the bands disperse from $\overline{\Gamma}$ and $\overline{M}$, forming only one Dirac cone at $\overline{\Gamma}$. For doped thick films (e.g., 100 BL), the band is nontrivial, same as the semi-infinite surface. For doped thin films (<100

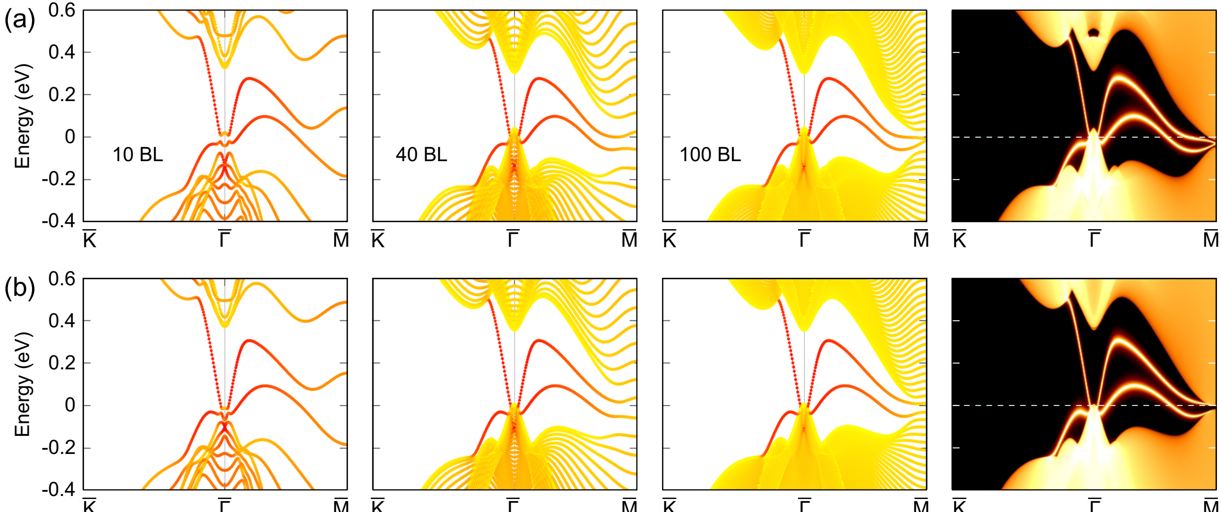

FIG. 4. (a) Calculated surface band structures of 10 BL, 40 BL, and 100 BL films and semi-infinite surface for intrinsic Bi indicating a HOTI. (b) Calculated surface band structures of 10 BL, 40 BL, and 100 BL films and semi-infinite surface for $\Delta n = 0.98 \times 10^{-4}/\text{Å}^3$ ($\Delta V = 2.8\%$) indicating a TI.

BL), the tunneling effect between the two surfaces opens gaps in the surface bands at the TRIM points, particularly the $\overline{M}$ point, which alters the connection between the surface band to the bulk conduction and valence bands. Due to the small gap at the L point ($\sim$10 meV), the band dispersion for thinner doped thin films (10 BL and 40 BL) is seen to be indistinguishable between the HOTI and TI phase, i.e., one surface branch merges into a valence and the other into a conduction band. In other words, the small gap of Bi requires a thick film (>100 BL) to remove the coupling between the up and down surface Dirac state. Consequently, at the thin film limits, it is hard to distinguish the topological order by only examining surface bands. Alternatively, one has to look into other factors, such as doping (shift of Fermi level) and lattice strain as we do here.

Remarkably, we are able to resolve all the outstanding discrepancies among the existing experiments and theories on the topological nature of bulk Bi, in light of the effects of electron doping and lattice expansion. For example, in one system where the topological surface state is observed, it is

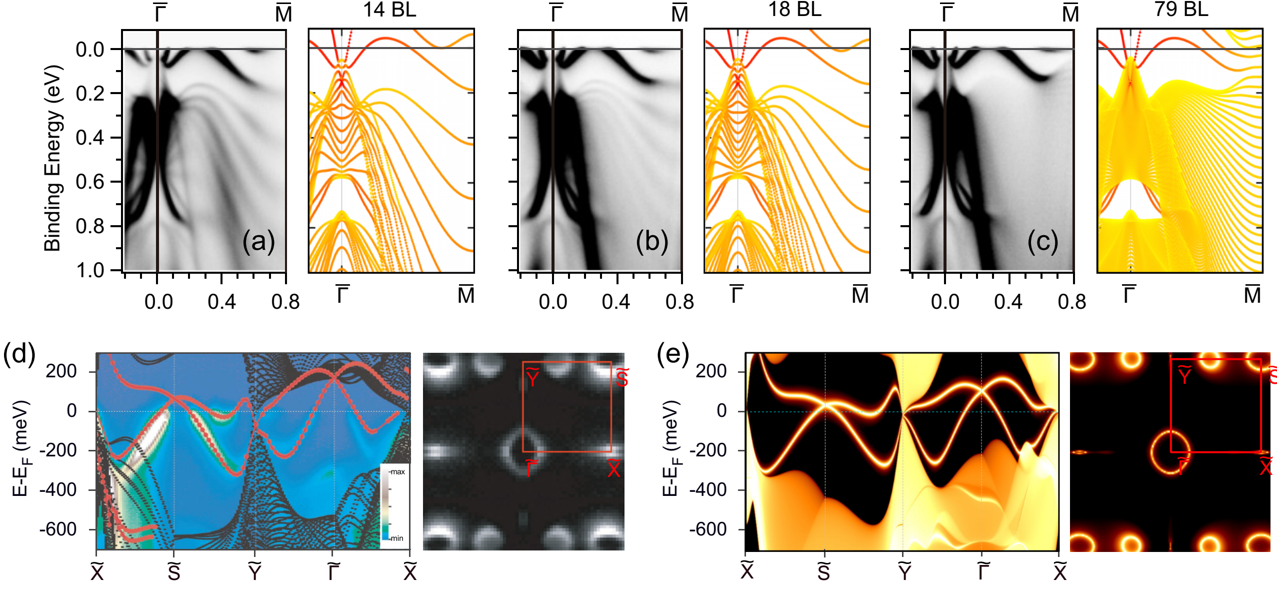

FIG. 5. (a)–(c) Comparison of DFT surface state of Bi (111) thin films ($\Delta n = 0.98 \times 10^{-4}/\text{Å}^3$ and $\Delta V = 2.8\%$) for 14 BL, 18 BL, and 79 BL with experimental ARPES results (left panel), respectively. The experimental images were taken from Ref. [32]. The experimental Fermi level was set to zero. The calculated surface states have been shifted downward (i.e., Fermi level shift upward) by 0.05 eV for electron doping to match with ARPES data within the rigid-band approximation. The nontrivial character of surface states is well reproduced. (d) Experimental ARPES and Fermi surface for Bi (110) surface states which were taken from Refs. [52,53]. (e) Calculated surface states and Fermi surface of Bi (110) semi-infinite surface. For Bi (110) surface states, we used Wannier fitting parameters of the equilibrium structure of Bi bulk ($\Delta n = 0$). To match with experimental ARPES data, no need to shift Fermi level for Bi (110) surface.

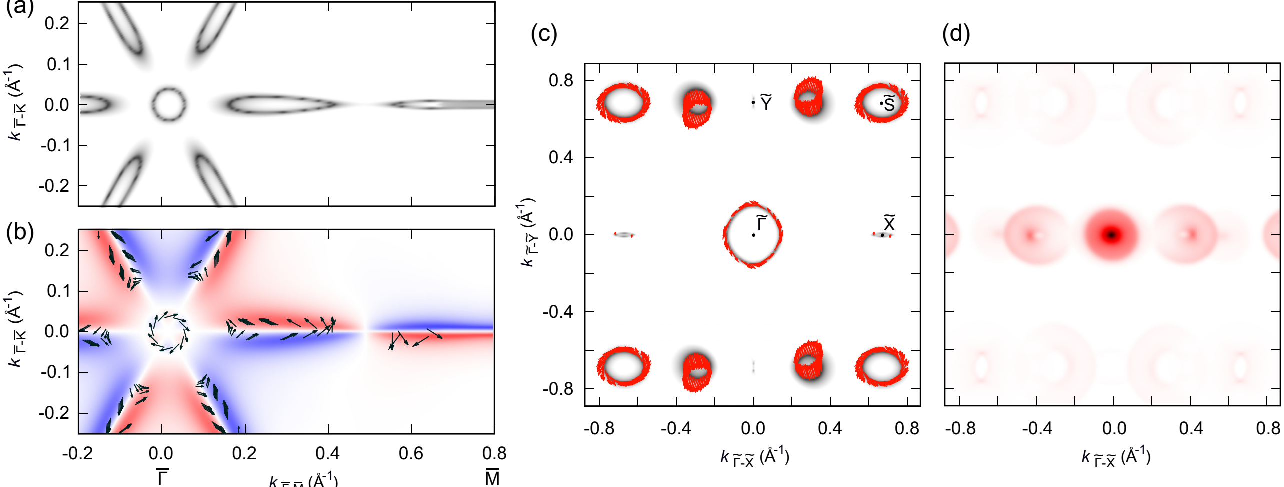

FIG. 6. (a) and (b) The Fermi surface of semi-infinite Bi (111) films ($\Delta n = 0.98 \times 10^{-4}/\text{Å}^3$ and $\Delta V = 2.8\%$) and corresponding spin textures, respectively. The arrows (with red/blue background) indicate the in-plane (out-of-plane) spin component. (c) and (d) The calculated spin texture of Bi (110) semi-infinite surface ($\Delta n = 0$) and the QPI pattern at the Fermi level, respectively.

reported that the Bi (111) film has ~3% interlayer expansion [54] which is sufficient to induce a topological HOTI-to-TI phase transition [see Fig. 3(c)]. To make a direct comparison, we have calculated the surface states of the Bi (111) thin films of different thickness with $\Delta n = 0.98 \times 10^{-4}/\text{Å}^3$, as shown in Figs. 5(a)–5(c). To match with experimental results, we found the calculated bands have to be shifted by −0.05 eV (electron doping) [Fig. 2(d)]. Then the calculated surface states agree well with the recent ARPES measurements [32]. By using the strained Bi film that corresponds to this amount of doping, the calculated topological surface states emerge, with one branch merging into a valence and the other into a conduction band near the $\overline{M}$ point, in very good agreement with the ARPES data. Thus, based on the Fermi energy shift ($\Delta E_F = 0.05$ eV) and the amount of strain needed to match the experimental data, we deduce that the experimental Bi (111) films [32] is likely to be electron doped with a ~3% lattice expansion induced by QES. In particular, the shifting of $\Delta E_F = 0.05$ eV corresponds to an electron doping level $\Delta n \sim 1.1 \times 10^{-4}/\text{Å}^3$ [Fig. 2(d)] and the system should be a TI according to Fig. 3(c). On the other hand, the experimental ARPES data of Bi (110) surface states [52,53] are compared with the calculated surface states of Bi (110) at the equilibrium lattice without doping [Figs. 5(d) and 5(e)]. In this case, a Fermi level shift is not needed to match with the experimental ARPES data, indicating that there is no doping-induced QES effect on the Bi (110) surface, and the system is a HOTI.

In addition to comparing with experimental ARPES data, we also checked the spin states of bismuth films. Figures 6(a) and 6(b) show the calculated Fermi surface and corresponding surface spin texture of semi-infinite Bi (111) surface ($\Delta n = 0.98 \times 10^{-4}/\text{Å}^3$ and $\Delta V = 2.8\%$). There is an isotropic electron pocket at the $\overline{\Gamma}$ point, and six anisotropic hole and extra electron pockets along the $\overline{\Gamma}$-$\overline{M}$ direction. The arrows in Fig. 6(b) show the in-plane spin distribution. In the electron pocket around the $\overline{\Gamma}$ point, spin lies in the (k_x, k_y) plane with a helical spin texture due to the TI order. While in the other hole or electron pockets, a large out-of-plane spin component appears. Moreover, the out-of-plane spin polarization switches the sign across the $\overline{\Gamma}$-$\overline{M}$ line. These observations are consistent with previous experimental results [55–58]. Figure 6(c) shows the spin texture of semi-infinite Bi (110) surface ($\Delta n = 0$). There are two hole pockets at the $\widetilde{\Gamma}$ and $\widetilde{S}$ points [Figs. 5(e) and 6(c)], and a shallow electron pocket centered somewhere along the $\widetilde{Y}$-$\widetilde{S}$ line [53]. The spin directions on the Fermi surface are indicated by red arrows. Most of spins are oriented in-plane, and the spin helicity is same for the two hole pockets at the $\widetilde{\Gamma}$ and $\widetilde{S}$ points. On the other hands, the spins of electron pockets are aligned along the $\widetilde{\Gamma}$-$\widetilde{Y}$ direction. The calculated quasiparticle interference (QPI) spectra are shown in Fig. 6(d), which contain the fingerprints of the scattering process of surface states due to their unique spin texture.

IV. CONCLUSION

In conclusion, we have demonstrated a TPT induced by QES that depends on electron/hole doping. Using this idea we resolve the outstanding controversy regarding the topology of bulk and thin-film Bi. Generally, by accounting for the electron doping-induced QES and hence anisotropic lattice expansion, all the existing experiments and theories can be reconciled in good agreement. We expect the effect of QES to manifest broadly in the doped small-gap topological insulating materials and in turn would provide extra controllability over their topological property.

ACKNOWLEDGMENTS

This work was supported by DOE-BES (Grant No. DE-FG02-04ER46148). K.J. acknowledges the support from Korea Research Fellowship Program through the National Research Foundation of Korea (NRF) funded by the Ministry of Science and ICT (Grant No. 2019H1D3A1A01071056). The calculations were done on the CHPC at the University of Utah and NERSC of DOE.

[1] H. J. Queisser and E. E. Haller, Science **281**, 945 (1998).
[2] M. D. Mccluskey and E. E. Haller, *Dopants and Defects in Semiconductors* (CRC, Boca Raton, FL, 2012).
[3] N. P. Armitage, P. Fournier, and R. L. Greene, Rev. Mod. Phys. **82**, 2421 (2010).
[4] K. E. Wagner, E. Morosan, Y. S. Hor, J. Tao, Y. Zhu, T. Sanders, T. M. McQueen, H. W. Zandbergen, A. J. Williams, D. V. West, and R. J. Cava, Phys. Rev. B **78**, 104520 (2008).
[5] G. Profeta, M. Calandra, and F. Mauri, Nat. Phys. **8**, 131 (2012).
[6] C. Si, Z. Liu, W. Duan, and F. Liu, Phys. Rev. Lett. **111**, 196802 (2013).
[7] Y. S. Hor, A. J. Williams, J. G. Checkelsky, P. Roushan, J. Seo, Q. Xu, H. W. Zandbergen, A. Yazdani, N. P. Ong, and R. J. Cava, Phys. Rev. Lett. **104**, 057001 (2010).
[8] L. A. Wray, S.-Y. Xu, Y. Xia, Y. S. Hor, D. Qian, A. V. Fedorov, H. Lin, A. Bansil, R. J. Cava, and M. Z. Hasan, Nat. Phys. **6**, 855 (2010).
[9] Y. L. Chen, J. G. Analytis, J.-H. Chu, Z. K. Liu, S.-K. Mo, X. L. Qi, H. J. Zhang, D. H. Lu, X. Dai, Z. Fang, S. C. Zhang, I. R. Fisher, Z. Hussain, and Z.-X. Shen, Science **325**, 178 (2009).
[10] D. Hsieh, Y. Xia, D. Qian, L. Wray, J. H. Dil, F. Meier, J. Osterwalder, L. Patthey, J. G. Checkelsky, N. P. Ong, A. V. Fedorov, H. Lin, A. Bansil, D. Grauer, Y. S. Hor, R. J. Cava, and M. Z. Hasan, Nature (London) **460**, 1101 (2009).
[11] M. Neupane, S. Y. Xu, L. A. Wray, A. Petersen, R. Shankar, N. Alidoust, C. Liu, A. Fedorov, H. Ji, J. M. Allred, Y. S. Hor, T. R. Chang, H. T. Jeng, H. Lin, A. Bansil, R. J. Cava, and M. Z. Hasan, Phys. Rev. B **85**, 235406 (2012).
[12] Z. F. Wang, Z. Liu, and F. Liu, Nat. Commun. **4**, 1471 (2013).
[13] S. Murakami, Phys. Rev. Lett. **97**, 236805 (2006).
[14] F. Yang, L. Miao, Z. F. Wang, M.-Y. Yao, F. Zhu, Y. R. Song, M.-X. Wang, J.-P. Xu, A. V. Fedorov, Z. Sun, G. B. Zhang, C. Liu, F. Liu, D. Qian, C. L. Gao, and J.-F. Jia, Phys. Rev. Lett. **109**, 016801 (2012).
[15] S. H. Kim, K.-H. Jin, J. Park, J. S. Kim, S.-H. Jhi, T.-H. Kim, and H. W. Yeom, Phys. Rev. B **89**, 155436 (2014).
[16] F. Reis, G. Li, L. Dudy, M. Bauernfeind, S. Glass, W. Hanke, R. Thomale, J. Schäfer, and R. Claessen, Science **357**, 287 (2017).
[17] H. Hu, M. Liu, Z. F. Wang, J. Zhu, D. Wu, H. Ding, Z. Liu, and F. Liu, Phys. Rev. Lett. **109**, 055501 (2012).
[18] H. Fukuyama and R. Kubo, J. Phys. Soc. Jpn. **28**, 570 (1970).
[19] K. Behnia, L. Balicas, and Y. Kopelevich, Science **317**, 1729 (2007).
[20] O. Prakash, A. Kumar, A. Thamizhavel, and S. Ramakrishnan, Science **355**, 52 (2017).
[21] J. C. Y. Teo, L. Fu, and C. L. Kane, Phys. Rev. B **78**, 045426 (2008).
[22] S. Golin, Phys. Rev. **166**, 643 (1968).
[23] X. Gonze, J. P. Michenaud, and J. P. Vigneron, Phys. Rev. B **41**, 11827 (1990).
[24] Y. Liu and R. E. Allen, Phys. Rev. B **52**, 1566 (1995).
[25] Y. M. Koroteev, G. Bihlmayer, J. E. Gayone, E. V. Chulkov, S. Blügel, P. M. Echenique, and P. Hofmann, Phys. Rev. Lett. **93**, 046403 (2004).
[26] I. Aguilera, C. Friedrich, and S. Blügel, Phys. Rev. B **91**, 125129 (2015).
[27] F. Schindler, Z. Wang, M. G. Vergniory, A. M. Cook, A. Murani, S. Sengupta, A. Y. Kasumov, R. Deblock, S. Jeon, I. Drozdov, H. Bouchiat, S. Guéron, A. Yazdani, B. A. Bernevig, and T. Neupert, Nat. Phys. **14**, 918 (2018).
[28] C. R. Ast and H. Höchst, Phys. Rev. B **67**, 113102 (2003).
[29] Y. Ohtsubo, L. Perfetti, M. O. Goerbig, P. L. Fèvre, F. Bertran, and A. Taleb-Ibrahimi, New J. Phys. **15**, 033041 (2013).
[30] H. M. Benia, C. Straßer, K. Kern, and C. R. Ast, Phys. Rev. B **91**, 161406(R) (2015).
[31] M.-Y. Yao, F. Zhu, C. Q. Han, D. D. Guan, C. Liu, D. Qian, and J.-f. Jia, Sci. Rep. **6**, 21326 (2016).
[32] S. Ito, B. Feng, M. Arita, A. Takayama, R. Y. Liu, T. Someya, W. C. Chen, T. Iimori, H. Namatame, M. Taniguchi, C. M. Cheng, S. J. Tang, F. Komori, K. Kobayashi, T. C. Chiang, and I. Matsuda, Phys. Rev. Lett. **117**, 236402 (2016).
[33] N. Shimamura, K. Sugawara, S. Sucharitakul, S. Souma, K. Iwaya, K. Nakayama, C. X. Trang, K. Yamauchi, T. Oguchi, K. Kudo, T. Noji, Y. Koike, T. Takahashi, T. Hanaguri, and T. Sato, ACS Nano **12**, 10977 (2018).
[34] H. Hu, H. Ding, and F. Liu, Sci. Rep. **5**, 8212 (2015).
[35] Z. Liu, C.-X. Liu, Y.-S. Wu, W.-H. Duan, F. Liu, and J. Wu, Phys. Rev. Lett. **107**, 136805 (2011).
[36] H. Weng, X. Dai, and Z. Fang, Phys. Rev. X **4**, 011002 (2014).
[37] K.-H. Jin, H. W. Yeom, and S.-H. Jhi, Phys. Rev. B **93**, 075308 (2016).
[38] G. Kresse and J. Furthmüller, Phys. Rev. B **54**, 11169 (1996).
[39] J. P. Perdew, K. Burke, and M. Ernzerhof, Phys. Rev. Lett. **77**, 3865 (1996).
[40] A. Tkatchenko and M. Scheffler, Phys. Rev. Lett. **102**, 073005 (2009).
[41] A. D. Becke and E. R. Johnson, J. Chem. Phys. **124**, 221101 (2006).
[42] F. Tran and P. Blaha, Phys. Rev. Lett. **102**, 226401 (2009).
[43] J. Heyd, G. E. Scuseria, and M. Ernzerhof, J. Chem. Phys. **118**, 8207 (2003).
[44] A. A. Mostofi, J. R. Yates, G. Pizzi, Y.-S. Lee, I. Souza, D. Vanderbilt, and N. Marzari, Comput. Phys. Commun. **185**, 2309 (2014).
[45] M. P. L. Sancho, J. M. L. Sancho, and J. Rubio, J. Phys. F **14**, 1205 (1984).
[46] Q. Wu, S. Zhang, H.-F. Song, M. Troyer, and A. A. Soluyanov, Comput. Phys. Commun. **224**, 405 (2018).
[47] P. Hofmann, Prog. Surf. Sci. **81**, 191 (2006).
[48] D. Schiferl and C. S. Barrett, J. Appl. Crystallogr. **2**, 30 (1969).
[49] A. J. Lichnowski and G. A. Saunders, J. Phys. C **9**, 927 (1976).
[50] B. Arnaud, S. Lebègue, and G. Raffy, Phys. Rev. B **93**, 094106 (2016).
[51] L. Fu and C. L. Kane, Phys. Rev. B **76**, 045302 (2007).
[52] S. Agergaard, C. Søndergaard, H. Li, M. B. Nielsen, S. V. Hoffmann, Z. Li, and P. Hofmann, New J. Phys. **3**, 15 (2001).
[53] J. I. Pascual, G. Bihlmayer, Yu. M. Koroteev, H.-P. Rust, G. Ceballos, M. Hansmann, K. Horn, E. V. Chulkov, S. Blügel, P. M. Echenique, and Ph. Hofmann, Phys. Rev. Lett. **93**, 196802 (2004).
[54] T. Hirahara, N. Fukui, T. Shirasawa, M. Yamada, M. Aitani, H. Miyazaki, M. Matsunami, S. Kimura, T. Takahashi, S. Hasegawa, and K. Kobayashi, Phys. Rev. Lett. **109**, 227401 (2012).
[55] T. K. Kim, J. Wells, C. Kirkegaard, Z. Li, S. V. Hoffmann, J. E. Gayone, I. Fernandez-Torrente, P. Häberle, J. I. Pascual, K. T. Moore, A. J. Schwartz, H. He, J. C. H. Spence, K. H. Downing,

S. Lazar, F. D. Tichelaar, S. V. Borisenko, M. Knupfer, and P. Hofmann, Phys. Rev. B **72**, 085440 (2005).

[56] T. Hirahara, T. Nagao, I. Matsuda, G. Bihlmayer, E. V. Chulkov, Y. M. Koroteev, P. M. Echenique, M. Saito, and S. Hasegawa, Phys. Rev. Lett. **97**, 146803 (2006).

[57] T. Hirahara, T. Nagao, I. Matsuda, G. Bihlmayer, E. V. Chulkov, Y. M. Koroteev, and S. Hasegawa, Phys. Rev. B **75**, 035422 (2007).

[58] A. Takayama, T. Sato, S. Souma, and T. Takahashi, Phys. Rev. Lett. **106**, 166401 (2011).